Absorbing capabilities of additively manufactured lattice structure specimens for crash applications: Damage tolerant design and simulations

Absorbing capabilities of Additively Manufactured lattice structure specimens for crash applications: damage tolerant design and simulations

Authors:
A. Tridello[a], C. Boursier Niutta[b], A. Benelli[c], D.S. Paolino[d]

[a] Department of Mechanical and Aerospace Engineering, Politecnico di Torino, 10129 Turin, Italy, andrea.tridello@polito.it
[b] Department of Mechanical and Aerospace Engineering, Politecnico di Torino, 10129 Turin, Italy, carlo.boursier@polito.it
[c] Department of Applied Science and Technology, Politecnico di Torino, 10129 Turin, Italy, alessandro.benelli@polito.it
[d]Department of Mechanical and Aerospace Engineering, Politecnico di Torino, 10129 Turin, Italy, davide.paolino@polito.it

Corresponding Author:
A. Tridello
E-mail address: andrea.tridello@polito.it
Full postal address:
C.so Duca degli Abruzzi 24,
Department of Mechanical and Aerospace Engineering – Politecnico di Torino,
10129 – Turin,
ITALY
Phone number: +39.011.090.6913
Fax number: +39.011.090.6999

Abstract:

In the present work, the influence of defects on the compressive response of octet-truss AlSi10Mg lattice structure specimens produced with a Selective Laser Melting process is investigated. The defect population in one cell, in two cells and cubic specimens composed of 27 cells has been assessed with micro-Computed Tomography (micro-CT) analyses. The statistical distributions of the characteristic defect sizes, i.e., the equivalent diameter, the volume and the surface, assessed on the lattice structure specimen and in volume randomly extracted from a rectangular bar have been compared. Finally, the compressive behaviour of lattice structure specimens has been simulated with a simplified damage-tolerant Finite Element model accounting for the influence of defects and compared with experimental results. The analyses have proven that the defect population in volumes extracted from a rectangular bar can provide reliable simulated results, even if micro-CT inspections of a unit cell or specimens made of several cells are suggested.

Keywords: Additive Manufacturing; Selective Laser Melting (SLM); lattice structures; AlSi10Mg alloy; crash; compressive response; structural integrity

Introduction

The increasing diffusion of components produced through Additive Manufacturing (AM) processes has boosted the research on the development of appropriate design strategies for these AM parts. The microstructure and defectivity of AM components are different from those of parts produced through traditional processes, like casting or machining [1–6], with implications on the structural integrity that cannot be ignored for a safe design. For example, many experimental results have confirmed that the fine microstructure resulting from repeated fusions in as-built Selective Laser Melting (SLM) or Electron Beam Melting (EBM) processes ensures a tensile strength close to that of parts produced with traditional manufacturing processes [7–9], with, on the other hand, a lower ductility [10–12]. Similarly, the fatigue life of AM parts tends to be lower than that of Traditionally Built (TB) components, mainly due to the high surface roughness [13–15], residual stresses [16,17] and the formation of large defects during the manufacturing process [18–20]. This analysis proves that traditional design methodologies, even if based on a "damage tolerance approach", may be not safe when applied to AM parts and that their effectiveness should be carefully verified and experimentally validated. This subject of research on the structural integrity of AM parts is therefore of utmost interest for ensuring their diffusion and their safe application.

Furthermore, the research is also focusing on defining new approaches ensuring the structural integrity of components which can be produced only, or more efficiently, with AM processes and whose diffusion has recently increased, like components designed with Topology optimization (TO) algorithms [21–23] or components made with lattice structures [24–27]. Both lattice structures and TO components ensure efficient material exploitation for lightweight applications, with the final geometry tailored to withstand external loads. In particular, lattice structures are designed and manufactured with periodic repetition in the space of a unit cell. The type of unit cell (e.g., octet-truss, gyroid), the diameter of the truss in beam-based lattice structures, and the size of the unit cell can be optimized for the specific application to achieve the desired properties [28–31]. For example, lattice structure parts, if properly designed, have shown interesting absorbing properties in crash applications [32–35]. Lattice structures represent a clear example of the potential of AM and therefore the research on their mechanical properties is of interest within the scientific community [24,25,29,31,36]. Indeed, despite the above-mentioned advantages, there are still open issues concerning their structural integrity. Lattice structure parts after the AM process show significant differences with respect to the ideal geometry provided in input to the AM process, due to the high resulting roughness or the presence of defects within the beam [15,37,38]. This irregular geometry and material defectiveness have a strong influence on the mechanical properties and must be necessarily taken into account with appropriate design methodologies, based on Finite Element Analyses (FEAs) and damage tolerance approaches [39].

For example, in the review paper [37] the Authors pointed out the importance of accounting for the influence of defects in numerical models ("*The incorporation of potential imperfections is a must to develop a model that reflects the actual response of a cellular structure*") and that micro-Computed Tomography (micro-CT) inspection is the most effective technique for assessing the defect population, despite its high cost. In [40], circular defects, with radius in the range $[20 - 60]\ \mu m$ and sinusoidal surface roughness, are simulated in inclined struts of Body Centered Cubic (BCC) lattice structures. The numerical results showed an exponential degradation of the mechanical properties, within thinner struts characterized by a more accentuated degradation. In [41], a methodology to correct the quasi-static properties of PA-12 lattice pillars produced with the SLS technology is proposed. In particular, the strut diameter to be considered in simulations is reduced two times, starting from Scanning Electron Microscope (SEM) analyses and numerical simulations. Firstly, the diameter is reduced by a first factor which accounts for the skin of the cross-section, corresponding to an improper fusion of the outer layer, which does not contribute to withstand the applied load. The second correction factor, on the other hand, accounts for the influence of internal porosities, by analysing the volume of defects. In [42], micro-CT inspections are carried out to assess the variability of mechanical properties due to defects, focusing on the deviation of the strut diameter. An interesting result is that the failure mode changes

depending on the defect density, i.e. a localized failure followed by crushing for lattice structures with a high density of defects and a 45° degree oriented failure in specimens with small defect density. In the compressive response of AlSi10Mg octet-truss lattice structure specimens produced with an SLM process is simulated. One-dimensional beam elements have been considered in the simulation, with the influence of the defect size accounted for by reducing the diameter of the beam starting from the defect distribution assessed with micro-CT inspections. This approach has proven to properly work and has been experimentally validated [43], providing a reliable and efficient "damage tolerant" design approach.

Together with the damage tolerance approaches for simulating the response of lattice structure specimens, the methodologies for assessing the part defectiveness in lattice structures play also a key role. Micro-CT is the most effective technique and provides a large amount of information on the defect population and characteristics, which should be properly exploited. The choice of the characteristic defect size (e.g., defect area or defect volume) and how it affects the investigated mechanical property can be challenging. For example, the projected area of the defect in a plane perpendicular to the maximum applied stress, which properly works for fatigue investigations [14], can be hardly assessed for defects randomly distributed in beams with different orientations. Similarly, statistical analyses of the defect population have relevant importance and implications on the results of the FEAs and the consequent design of components, characterized by a size which is significantly larger than that of the laboratory specimens. At the same time, literature papers have pointed out that, regardless of the irregular morphology of defects and surface roughness, simplified damage-tolerant FE models are necessary to limit computational efforts.

The paper aims to address the above-discussed literature open issues on the structural integrity of lattice structure specimens. The proposed research activity starts from micro-CT analyses carried out on AlSi10Mg octet-truss lattice structure specimens produced with an SLM process. The defect populations in a specimen made of 27 cells, separately in each of the 27 unit cells belonging to the specimen, in 13 specimens made of 2 unit cells and in volumes extracted from a rectangular SLM AlSi10Mg bar have been analysed with micro-CT inspections. Starting from this detailed information on the defect population, statistical analyses have been carried out to investigate the influence of the number of cells on the defect volumes, defect surfaces and equivalent defect diameters and to investigate the statistical distribution of the largest defects. Finally, the influence of the defect characteristic sizes on the compressive response of lattice structure specimens has been verified with a simplified FEA modelling the influence of defects with the approach defined by the Authors in [43] and validated with experimental tests.

As discussed in the literature review, the influence of defects on the compressive response of lattice structure parts for crash-absorbing applications has been investigated in the literature, but further efforts are necessary to define reliable design methodologies for these complex structures. In particular, for a wide, diffusion of these structures, design methodologies should ensure a compromise between a good approximation of the experimental response and acceptable computational efforts. To this aim, the experimental variability induced by manufacturing defects should be accounted for, even with simplified models. Micro-CT inspections provide a large amount of information on the defect population and the appropriate defect feature, e.g., defect volume, surface or projected area, should be considered for a proper simulation in the simplified model. This paper aims to investigate the defect features which are more appropriate for modelling the influence of defects in a simplified FE model based on 1D elements, investigating also the variability induced by the internal defects, which cannot be neglected for a safe and reliable design.

2. MATERIALS AND METHODS

In this Section, the experimental activity is described in detail. In Section 2.1, the material characteristics and the geometry of the lattice structure specimens used for the experimental campaign are described. Section 2.2 focuses on the micro-CT inspections. In Section 2.3, the compression tests are described.

2.1 Lattice structure geometry, production process and compression tests

The experimental activity has been carried out on lattice structure specimens with an octet-truss unit cell, whose geometry is shown in Fig. 1a. This "stretch-dominated" geometry has been selected by the Authors in previous work [44] and ensures the highest absorbing capabilities among the other investigated unit cells, with a balance between the absorbed energy and the total mass. The nominal beam diameter is equal to 1.5 mm, verified with SEM analyses [43], and the cubic cell length is equal to 9 mm. Three specimens with 27 cells (cubic specimens with three cells per side) have been produced and considered for the experimental activity. The CAD geometry of the specimen is shown in Fig. 1b.

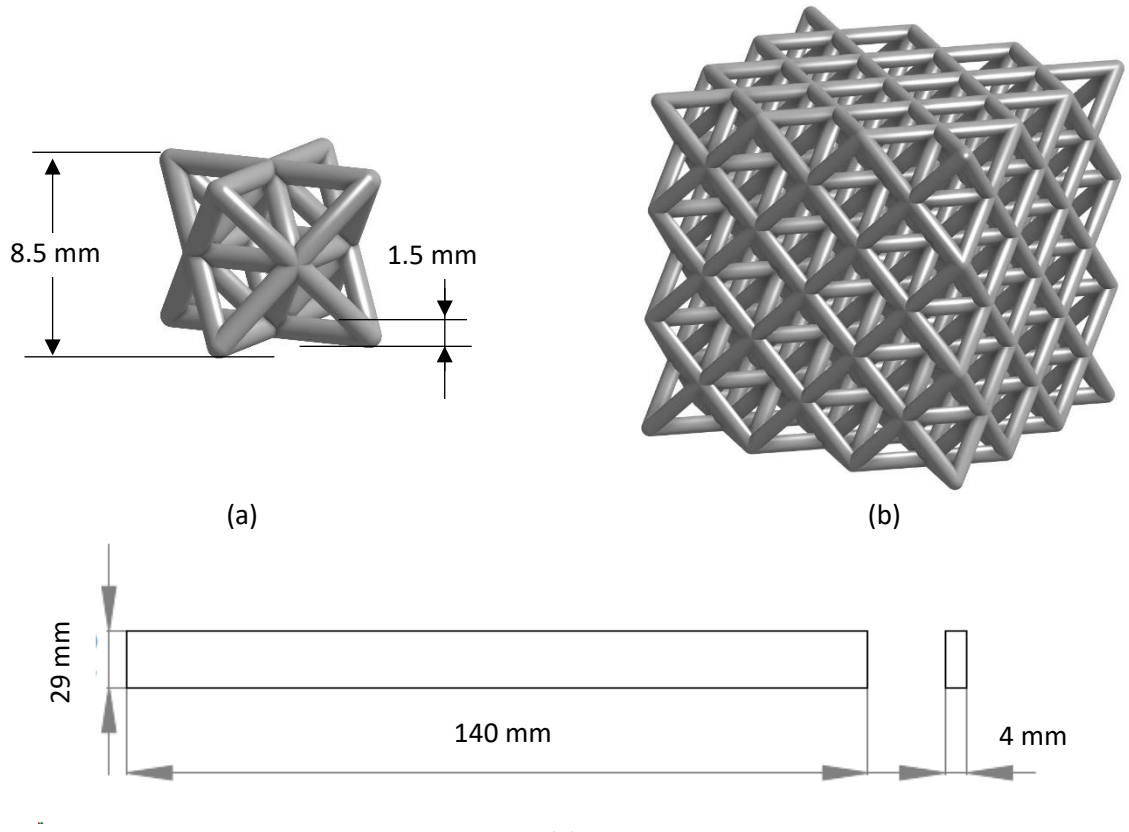

Figure 1: octet-truss lattice structure specimen investigated in the present paper: a) unit cell; b) 3x3 (27 cells) specimen geometry (not in scale); c) rectangular bar considered for the assessment of the defect population.

The specimens were produced with an SLM process by the Beam It industrial company and were made of an AlSi10Mg alloy. Table 1 summarizes the chemical composition of the investigated AlSi10Mg alloy specimens.

Si	Mg	Cu	Ni	Fe	Mn	Ti	Al
10	0.4	< 0.03	< 0.05	< 0.5	< 0.4	< 0.15	bal.

Table 1: chemical composition of the AlSi10Mg powder for the production of the investigated specimens (weight percentage, balance Aluminium).

The powder size, measured with the Laser Diffraction method, was characterized by an average value of $45\ \mu m$, with the 10% and 90% percentile equal to $33\ \mu m$ and $62\ \mu m$, respectively. The layer thickness was

set to $30\ \mu m$. After the AM process, the specimens were subjected to an aging treatment suggested by the specimen manufacturers and largely used in industrial applications, with a heating temperature of 200°C for 4 hours.

An AlSi10Mg rectangular bar with 29 x 4 mm cross-section and length equal to 140 mm (shown in Fig. 1c), produced with the same SLM process, was also inspected with micro-CT, according to the procedure detailed in the following Sections. The objective of this further analysis was to verify if the defect population obtained by inspecting a bar with simple geometry can be used in damage-tolerant numerical simulations (Section 4). This is certainly a simplification, since the defect population depends also on the final geometry to be produced. However, limited differences can be considered acceptable and would significantly simplify the design stage of the lattice structures, especially when large components with several cells are to be produced.

2.2 Micro-CT inspections and data analysis

X-ray CT analyses were carried out by using a custom-made system available in the J-Tech@PoliTO laboratories. The facility is equipped with a 300 kV X-ray source and a 5 µm minimum focal spot size, complemented by a flat panel detector featuring 2048 x 2048 pixels. The working distance between the source and the sample, as well as between the source and the detector, can be adjusted to obtain the highest resolution.

For the analysis of the specimens, the scanning parameters were optimized, with 170 kV and 100 µA resulting in an electron beam power of 17 W and achieving a final resolution of 25 µm per voxel. To enhance image quality, a physical filtering of 0.2 Cu was applied to the X-rays, effectively filtering out low-intensity radiation and minimizing noise in the subsequent reconstruction. During tomography acquisition, the distance between the X-ray source and the specimen was 100 mm while between the source and the detector was 1500 mm.

The reconstructed 3-D volume of the investigated specimens was obtained using the filtered back-projection algorithm through VG MAX 3.5 software (Volume Graphics GmbH, Heidelberg, DE), utilizing a total of 1600 X-ray projections. During post-processing, the porosity within the analysed specimens was meticulously detected and fully characterized, considering both dimensions and spatial distribution within the lattice structures. This comprehensive analysis provides valuable insights into the internal features of the specimens, contributing to a thorough understanding of their structural properties.

The micro-CT analyses were carried out on the three 3x3 lattice structure specimens and on volumes extracted from the rectangular bar to compare the defect population. In the following, the three 3x3 specimens will be referred to as “specimen 1”, “specimen 2” and “specimen 3”.

For the lattice structure specimens, different analyses were carried out by varying the number of considered cells. Firstly, all available specimens have been inspected. The volume of specimen 1 and specimen 2 was also discretized in sub-volumes to investigate the influence of the number of cells on the defect population. In particular, the total volume was subdivided into 27 unit cells. For specimen 1, the defect population in each unit cell was thereafter extracted (27 defect populations extracted). For specimen 2, the defect population in 2 cells was thereafter extracted (13 defect populations extracted). This procedure aims at replicating multiple micro-CT analyses on a unit cell (specimen 1) and two-unit cells (specimen 2). Fig. 2 shows an example of the specimen discretized into unit cells.

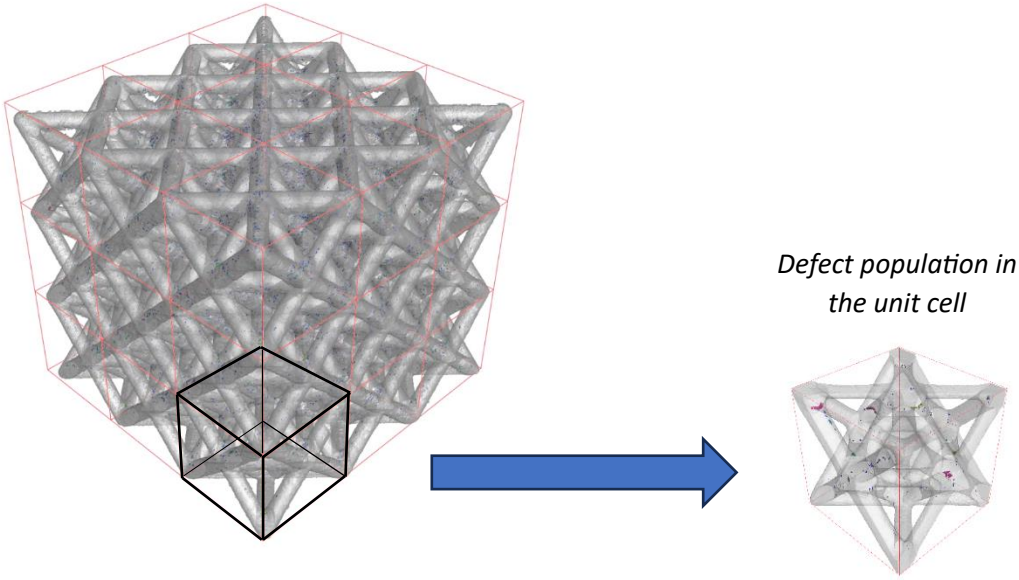

Figure 2: Example of micro-CT inspected lattice structure specimen discretized into sub-units.

Similarly, the rectangular bar was inspected with micro-CT and the inspected volume was discretized into smaller volumes with the same volume of a single unit cell. The sub-volumes were characterized by a fixed thickness, corresponding to the thickness of the bar, and a cross-section of 6100 µm x 6700 µm.

Table 2 summarizes the experimental activity carried out with micro-CT inspections.

Specimen type	**Analysis on the whole defect population**	**Analysis on the influence of the number of cells**
Lattice structures Specimen 1	Defect population within the whole volume	Defect population extracted in 27 unit cells, starting from the micro-CT inspection on the whole volume
Lattice structure Specimen 2	Defect population within the whole volume	Defect population in 13 cells, each one with a volume corresponding to the volume of two adjacent unit cells
Lattice structure Specimen 3	Defect population within the whole volume	-
Rectangular bar		12 micro-CT inspections on volumes corresponding to the volume of the unit cell

Table 2: summary of the micro-CT analyses carried out on the lattice structure specimens and the rectangular bar.

In damage-tolerant approaches, a characteristic defect size must be considered. The choice of this parameter is of fundamental importance in the subsequent FE analyses. To investigate how the results of the defect analysis and the FEAs are influenced by this parameter, three characteristic defect sizes are considered and compared in this analysis:

- Equivalent defect diameter, D_e: it corresponds to the diameter of a sphere which has the same volume of the defect.

- Defect surface: it corresponds to the surface area of the defect.
- Defect volume: it corresponds to the total volume of the defect.

2.3 Compression tests

Compression tests were carried out with a Zwick Roell Z100 electro-dynamic machine equipped with a 100 kN load cell. Displacement controlled, at a 1 mm/min crosshead speed, experimental tests were carried out on two 3x3 specimens with the same nominal geometry. During the experimental tests, together with the load signal, the specimen was recorded by using a Dino-Lite Digital Microscope to control the failure mode. It has been found that the specimens failed in correspondence of one of the corners and proceeded at 45° towards the opposite corner, which led to the abrupt decrease of the force signal. Thereafter, the densification phase initiated, with the force slowly increasing as the compression proceeded.

3. DEFECT ANALYSIS

In this Section, the results of the defect analysis are described and analysed in detail. In Section 3.1, the statistical method developed to analyze the defect population is described. In Section 3.2 details on the defect analysis with the Volume Graphics software are provided. In Section 3.3 the results of the defect analysis have been analysed in a statistical framework.

In this Section, the statistical distributions of the largest defect features and of the whole defect population are investigated. The Statistic of Extreme Values (SEV) is effectively employed for the assessment of the structural integrity of components failing from defects. Indeed, the largest defect is the one controlling the mechanical response and should be properly assessed. The choice of the defect feature to be considered for the application of the SEV is of fundamental importance to model the compressive response of lattice structures. The compressive response is mainly driven by the largest defect, but also other defects with smaller sizes can have an influence, depending on their location within the lattice cell. This is why the work has focused on the statistical distribution of the largest defects with the SEV, but also on the whole defect population and its statistical distribution.

3.1 Statistical distribution of the largest defects

In this Section, the procedure developed to analyse and compare the distribution of the largest defects from micro-CT inspections is described. Indeed, with micro-CT analyses, the entire population of defects is assessed. In the FE simulation of a compression test carried out in Section 4, the entire defect population is considered in the numerical model, with the location of the defect within the specimen randomly varied. Alternatively, when damage tolerance approaches are employed, design methodologies focus on the "extreme values", i.e., the largest and rare defects, which are those mostly affecting the structural integrity [45]. The largest defect characteristic size is assumed to follow the Largest Extreme Value Distribution (LEVD), and a "block maxima sampling" approach is generally followed to estimate the parameters of the LEVD [46]. According to this approach, the largest defect within a representative unit volume, V_0, is measured. This procedure is repeated for n available V_0 and these largest defects are then considered for the estimation of the parameters of the LEVD. However, when a micro-CT inspection is carried out on one specimen, only one volume is available and the LEVD cannot be estimated. One solution is to discretise the specimen volume in n_s subunits with volume V_{sub} and, for each sub-unit, to assess the largest defect. Accordingly, n_s largest defects are obtained and the LEVD for V_{sub} can be estimated. This procedure replicates a block maxima approach in the considered unit cell.

The LEVD for the whole specimen defect population can be alternatively obtained by replicating the block maxima approach according to the flow chart shown in Fig. 3, in which the equivalent defect diameter, D_e has been considered as an example. This methodology has been implemented with the numerical software Matlab®. Firstly, after the micro-inspection with subsequent defect analysis, the empirical cumulative distribution function (ECDF) of the D_e values is estimated with the Kaplan-Meier estimator. To account for the randomness associated with the estimation process, a randomly β_i confidence level ECDF has been considered. Thereafter, according to step 3 in Fig. 3, n_d random probability α values are generated and, for each α probability level, a random defect size D_e is estimated from the β_i confidence level ECDF (step 4). In step 5, the largest D_e among the n_d randomly estimated D_e is extracted. Steps 2 to 5 are then repeated n_{LEVD} times. At the end of step 6, n_{LEVD} defects are available for the estimation of the LEVD with the least square method, according to [46]. It must be noted that this procedure has been shown in Fig. 3 by considering the equivalent defect diameter, but it can be employed by considering other characteristic defect parameters (e.g., the defect volume, the defect surface), as in the analyses in Sections 3 and 4.

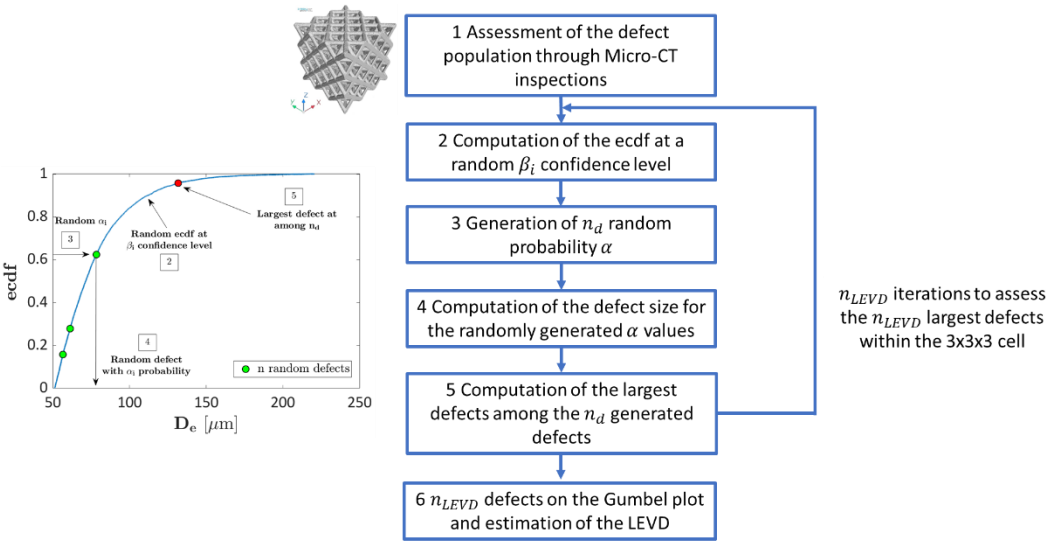

Figure 3: Workflow of the procedure developed for replicating a "block maxima approach" by considering the whole defect population obtained with a micro-CT inspection in the 3x3 lattice structure specimen.

3.2 Defect characteristics analysis

The software Volume Graphics has been used for the defect analysis. After the reconstruction of the specimen, the grey scale of each voxel is identified. Darker voxels correspond to materials with lower absorption of X-rays intensity which can be associated with voids inside the structure, being the samples made from a single material. For each defect, the algorithm provides a probability value strictly related to the difference in grey scale value between the possible defect and the surrounding material, i.e., the higher the difference, the higher the probability factor. Accordingly, defects with low probability levels are considered artefacts by the algorithm, caused by noise in the reconstruction process. Moreover, to discard surface defects, caused by the reconstruction noise, the algorithm searching distance has been limited to 25 µm away from the surface. Owing to the spatial resolution of the tomography system, which is 25 µm, the minimum detectable volume defect in the defect analysis is approximately 70000 µm³. According to the VG software manual, defects larger than four times the minimum detectable size should be considered for comprehensive analysis. While it is possible to detect defects of smaller sizes, there is an increased likelihood of error, as cautioned by the software manual. Moreover, defects with a volume smaller than 70000 µm³ are not

expected to affect the compressive response, since defects with a volume 100 times bigger are also present. Therefore, defects below this threshold volume have been excluded from the analysis. Indeed, the objective of the research activity is not to investigate all defects present in the specimens but to focus on those affecting the structural integrity, i.e., the largest defects. Therefore, excluding these defects facilitates the analysis and does not affect the following simulations, as verified in Section 4.

In Fig.4, all inspected volumes are reported. Fig. 4a shows the bar volume, Fig. 4b shows “specimen 1”, Fig. 4c shows “specimen 2” and Fig. 4d shows “specimen 3. The scale bar refers to all figures. The defects present in the investigated volumes are mostly lack of fusion defects or porosities, typical of parts produced with AM processes. However, a detailed analysis of the defect origin has not been carried out, since the objective of the paper is to investigate the defect feature which can be exploited for the assessment of the structural integrity of lattice structure specimens under compression loads, regardless of the defect origin. It is worth noting, however, that the information on the defect origin can be employed for optimizing the AM process and, therefore, to limit the occurrence of a specific typology of defects forming due to a non-optimized process, but this is out of the scope of the present work.

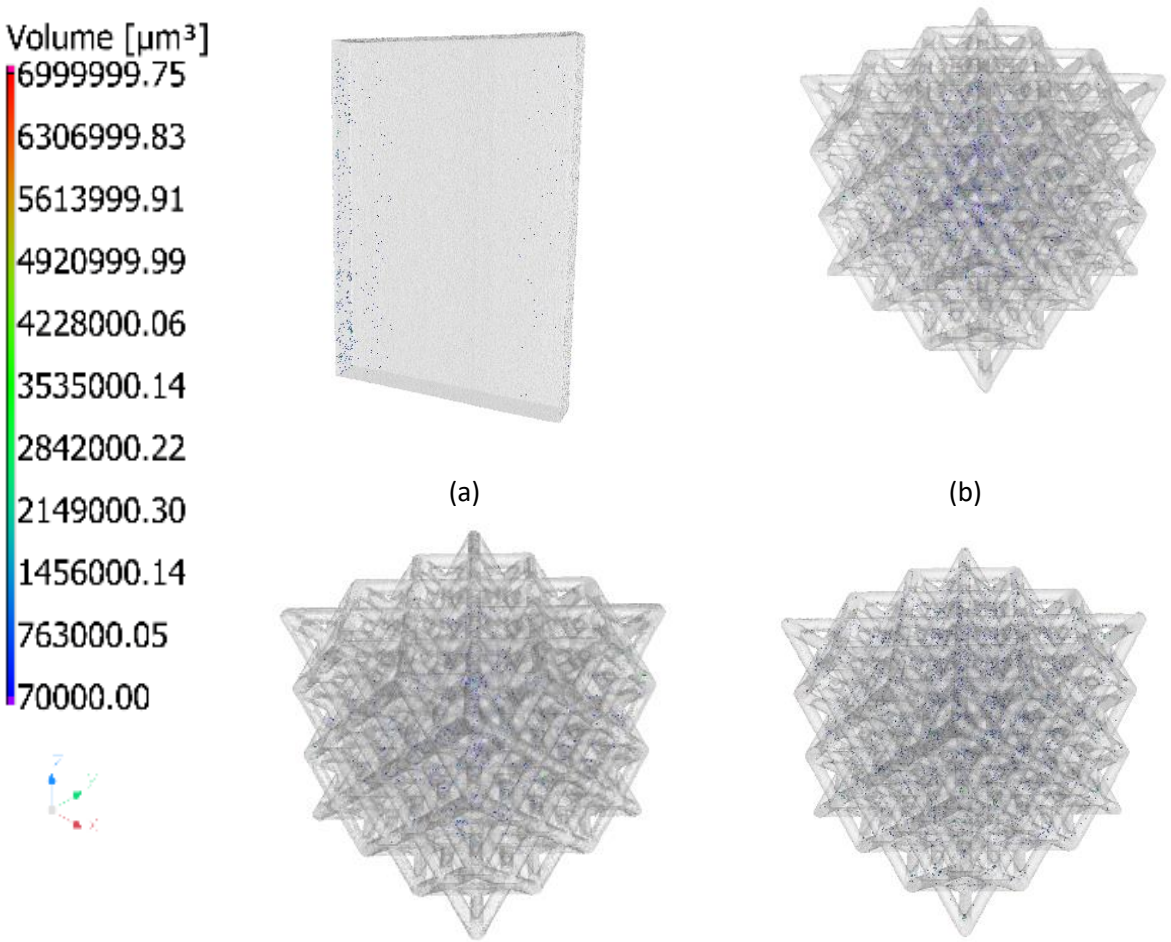

Figure 4: Representative images of the analysed samples and defect populations (the scale bar refers to all figures): a) rectangular bar; b) specimen 1; c) specimen 2; d) specimen 3.

According to Fig. 4, defects are randomly distributed within the bar and the lattice structure specimens. Small defects (coloured in blue) are mainly visible and occur with higher frequency. However, large but rare defects are present and they mostly affect the structural integrity of the part and have been carefully analysed in the next Section. The defect volume ratio, computed as the ratio between the defect volume and the specimen volume without defects, is equal to 0.01%, 0.01% and 0.053% for specimens 1, 2 and 3, respectively. However, rather than the total defect density, the density of large defects affects the mechanical response and should be taken into account. For example, the defect volume ratio by considering defects with equivalent diameter above the 50% of the largest defect is equal to 0.004%, 0.002% and 0.0018% (for specimens 1, 2 and 3, respectively) and reduces to 0.0001%, 0.0001% and 0.0004% (for specimens 1, 2 and 3, respectively) by considering defects with equivalent diameter above the 90% of the largest defect. These large and detrimental defects, characterized by a very small density, are those of greater importance for modelling the compressive response and have been analyzed in detail in the following sections.

According to Fig. 4a, larger defects are mainly concentrated close to the surface, with rarer internal large defects. The inspected volumes have been selected close to the surface since this is the condition of the struts in lattice structures, i.e., the volume of the lattice structure where defects form is mainly concentrated close to the surface layer due to their small diameter. Moreover, the external surface is the one with the largest defect density, thus the defect population assessed in this region is expected to provide results which are more conservative and therefore of greater relevance for design purposes and in a structural integrity context.

3.3 Statistical analysis of the defect population

In this Section, the defects found through micro-CT inspections are analysed in a statistical framework. The objective of this analysis is to compare the defect population assessed by investigating different numbers of cells and to verify how the results of the statistical analysis vary depending on the considered defect parameter, i.e., the equivalent diameter, the defect surface and the defect volume. Indeed, the square root of the projected area of the defect in a plane perpendicular to the direction of the maximum stress is commonly considered as the characteristic defect size in damage tolerance approaches [46]. However, in lattice structure specimens, beams with different orientations are present and, depending on the beam orientation, the direction of the maximum stress varies. Accordingly, it can be rather complex and time-consuming to assess the direction of the maximum stress for each defect, depending on its location, to verify how critical it is. In [45], a plane perpendicular to the direction of the applied load has been considered for assessing the characteristic defect size. Another possibility is to consider a defect size characteristic independent of the stress direction. For this reason, the defect volume, the defect surface and the equivalent diameter have been considered in this analysis, since they do not depend on the direction of the maximum stress and can be computed from micro-CT inspections. The choice of the appropriate defect characteristic is, however, fundamental for the design of lattice structure specimens, as verified and investigated in this and the following Section.

Fig. 5 compares the ECDF assessed by considering the defect volume (Fig. 5a), surface (Fig. 5b) and equivalent diameter (Fig. 5c) for the three investigated specimens and the bar. The total volume was considered in this analysis.

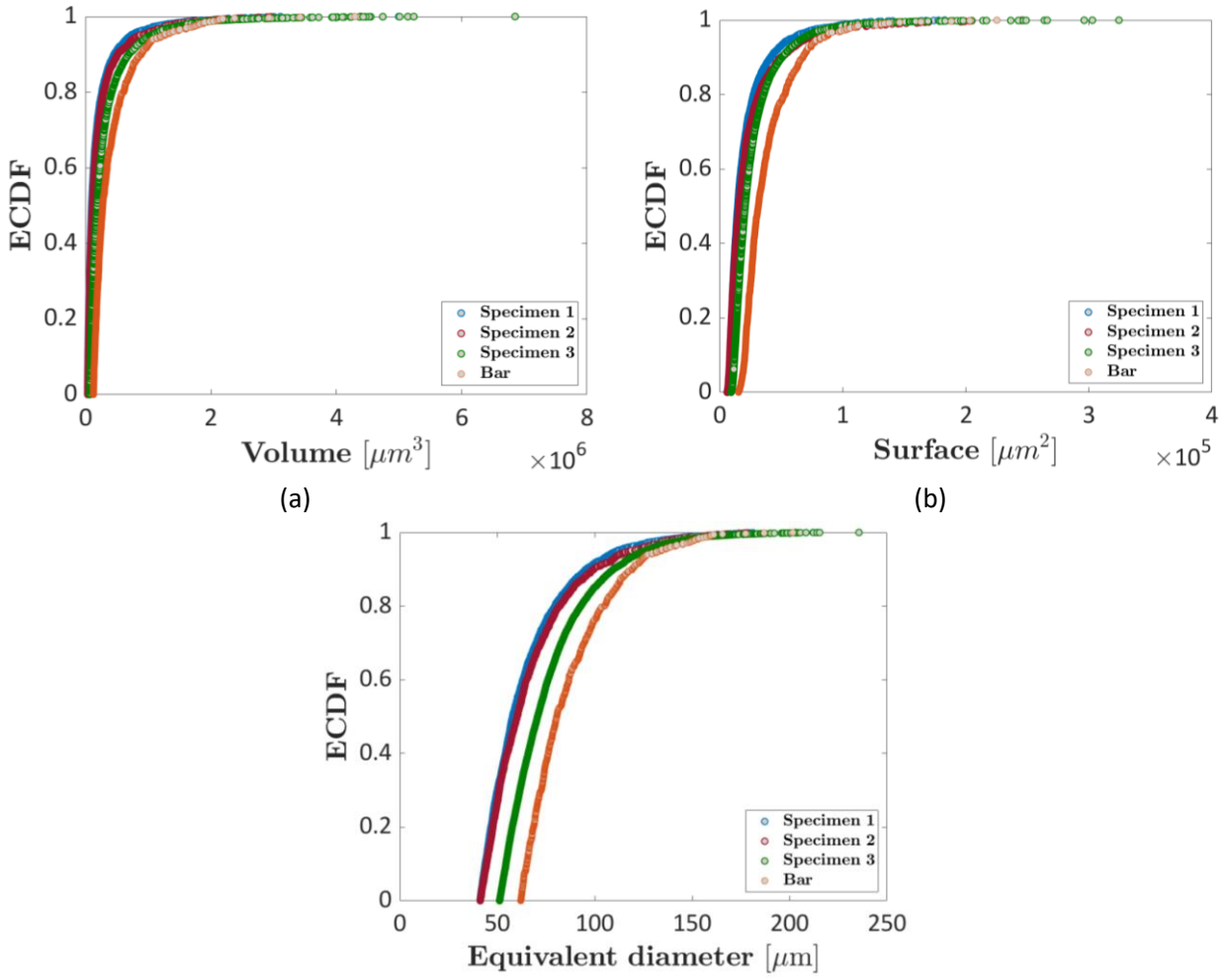

Figure 5: Empirical cumulative distribution function for the three investigated specimens: a) defect volume; b) defect surface; c) defect equivalent diameter.

According to Fig. 5, the trend of the ECDFs for the 3 specimens is similar, but specimen 3 is characterized by defects with larger equivalent diameter, volume and surface values. Slightly different trends can be observed by comparing the investigated characteristic defect sizes, i.e., the distance of the ECDF functions for the bar with respect to the other ECDF functions is limited when considering the defect volume and increases for the surface and the equivalent diameter. This can be attributed to the irregular and complex morphology of the defects in AM parts. For example, as shown in Fig. 6 for specimen 3, the defect with the largest volume may not correspond to the defect with the largest surface. In particular, Fig. 6a shows the defect with the largest volume, which is different from the defect with the largest surface, shown in Fig. 6b.

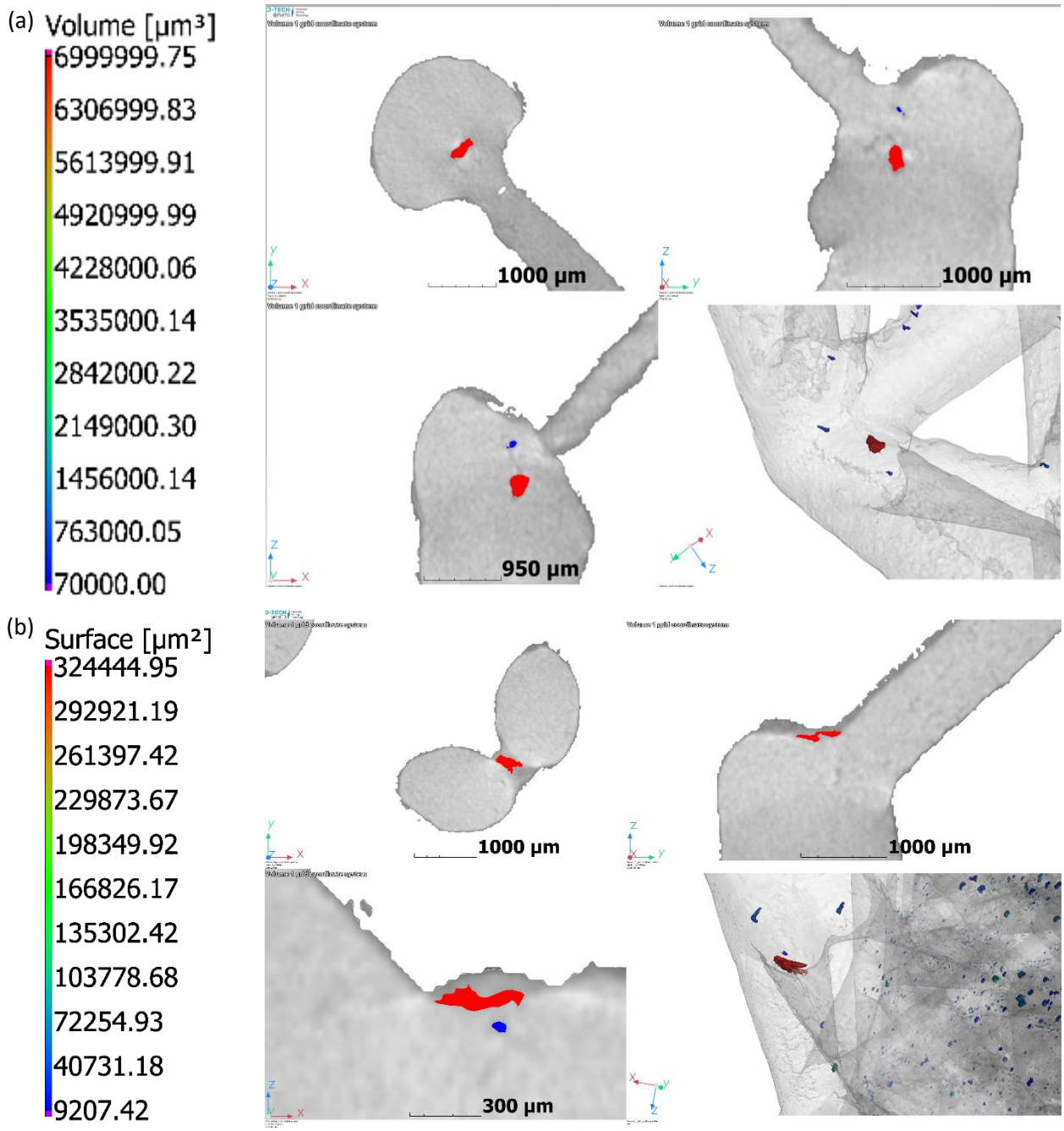

Figure 6: Largest defects obtained with porosity analysis for specimen 3: a) largest defect in terms of volume and b) largest defect in terms of surface.

Fig. 7, which plots the defect sphericity with respect to the defect volume (Fig. 7a), the defect surface (Fig. 7b) and the defect equivalent diameter (Fig. 7c) for specimen 3, confirms that the complex morphology of

defects in lattice structure parts requires proper investigations. Indeed, according to Fig. 7a and 7c, there is not a clear correlation between the defect sphericity and the defect volume or the equivalent diameter. On the other hand, the defect sphericity decreases with the defect surface, in agreement with literature results [47]. Therefore, depending on the considered parameters, the defect trend can vary and may affect the results of damage-tolerant FE simulation, as investigated in Section 4.

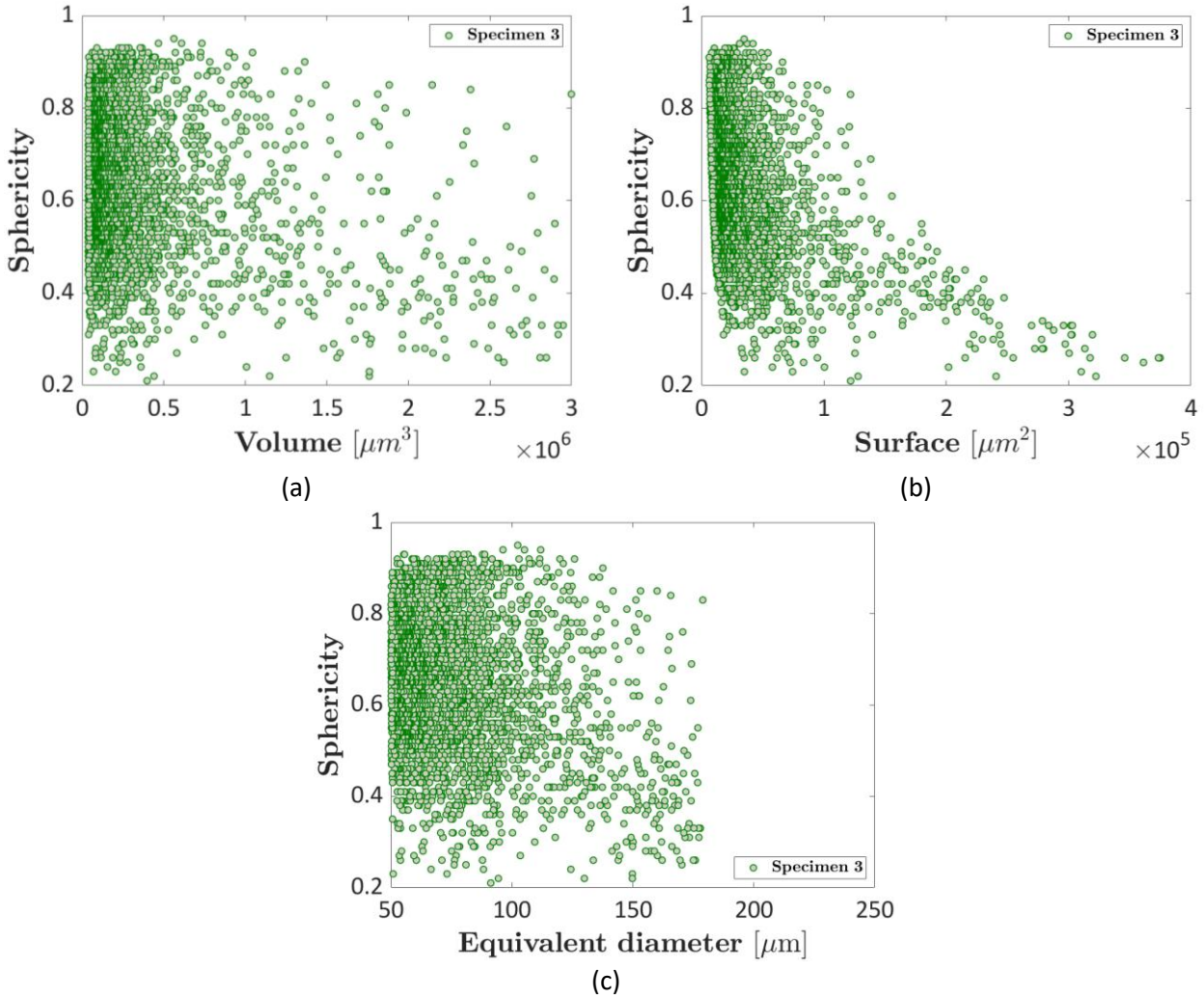

Figure 7: analysis of the defect sphericity for specimen 3: a) defect volume; b) defect surface; c) defect equivalent diameter.

In the following analyses, the statistical distributions of the defect size parameters and their variation with the number of available cells for micro-CT inspections are investigated. The defect population is generally assessed in specimens with a limited number of cells, but the number of cells in components can be significantly larger. The analyses have been carried out according to the plan detailed in Table 2, by comparing the defect population in a unit cell ("1 cell" in the following), in two cells ("2 cells" in the following) in the validation specimen ("3x3" specimen in the following) and in the volumes of the bar ("bar" in the following). According to the trends in Fig. 5 and Fig. 7, specimen 3 is considered the "validation specimen" since characterized by larger defects and therefore of major interest in a structural integrity framework.

Fig. 8a plots the ECDF functions of the defect volumes obtained by considering the 27 "1 cells", 13 "2 cells", the "3x3 specimen" and the "bar" volumes. The experimental ECDFs have been interpolated with a Piecewise Cubic Hermite Interpolating Polynomial (PCHIP) to avoid a stair-like appearance, especially for those volumes with a small number of defects. Fig. 8b plots the histogram of the defect volumes, with the box on the right

showing a magnified view of the upper tail of the histogram plot, to investigate the largest and most critical defects. Fig. 8c plots the largest defect volumes on the Gumbel plot. The experimental data obtained in the bar have been fitted with the LEVD, whereas the experimental data obtained in the "1 cell", the "2 cells" and the "3x3" specimens have been fitted with a Type 3 Generalized Extreme Value Distribution (GEVD, [48]), which considers an upper size defect volume limit, i.e., an asymptotic trend. In particular, the GEVD distribution has the following form:

$$G_\gamma(x) = exp\left\{-\left[1+\gamma\cdot\left(\frac{x-\mu}{\sigma}\right)\right]^{-\frac{1}{\gamma}}\right\}, \quad (1)$$

being x the defect characteristic size, μ the location parameter, σ the scale parameter and γ the shape parameter. The Type 3 GEVD is characterized by $\gamma < 0$, whereas for $\gamma \to 0$, the GEVD tends to a LEVD, also called Gumbel distribution. The choice of the fitting distribution for the investigated parameter will be discussed in the following. The parameter estimation has been carried out by applying the Maximum Likelihood Principle. In Fig. 8c, F_V is the cumulative distribution function (cdf) of largest defect volumes.

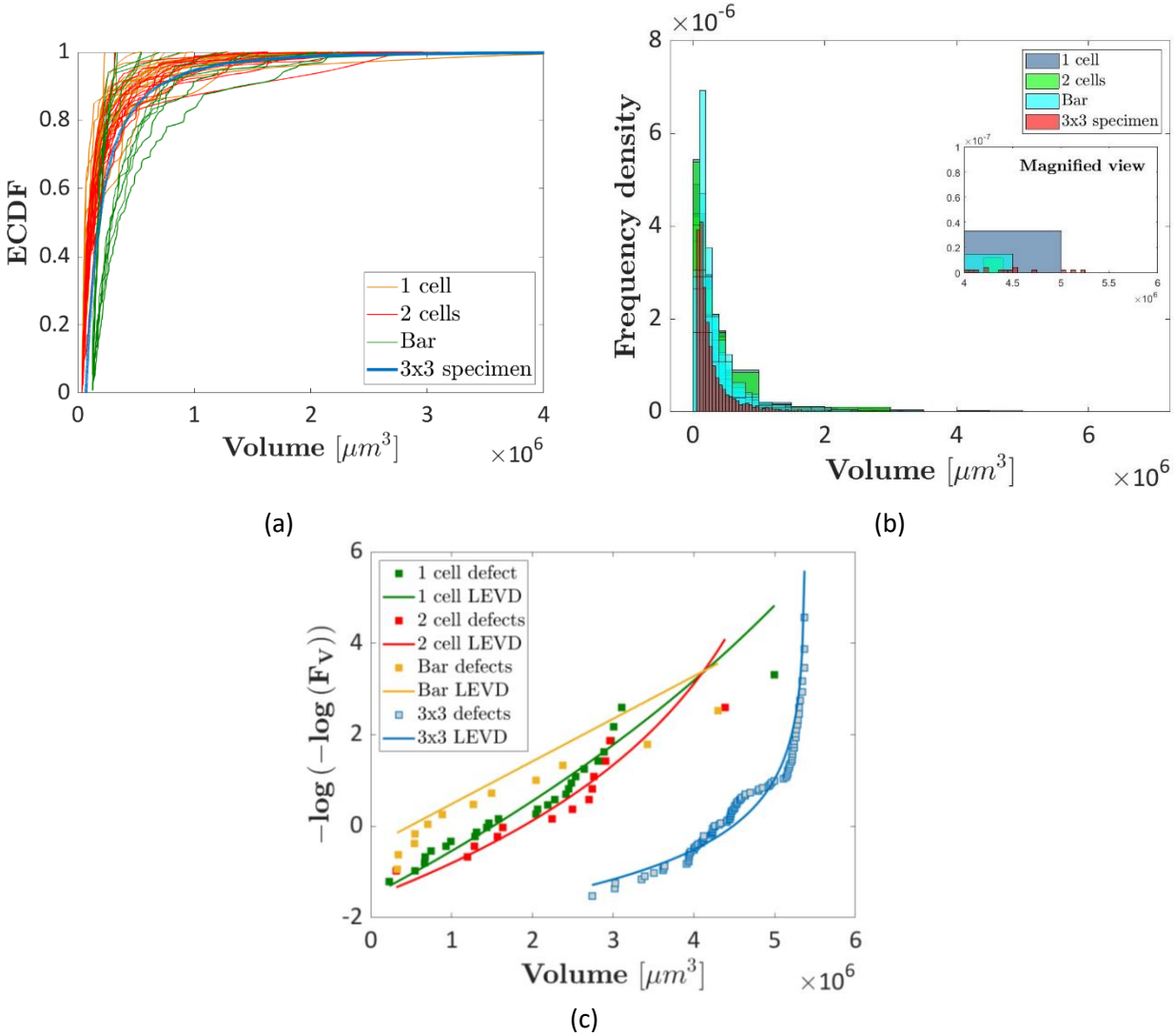

Figure 8: analysis of defect volumes: a) ECDF function of the defect volumes; b) histogram plot of the defect volumes; c) experimental data and estimated LEVD and Type 3 GEV functions on the Gumbel plot.

According to Fig. 8a, the trend of the ECDF functions is similar, as expected. The "1 cell", "2 cells" and "bar" defect volume ECDFs show more irregular trends, due to the possible limited defect numerosity in these small

investigated volumes. The ECDF for the 3x3 specimen is within the range of the ECDFs for “1 cell”, “2 cells” and “bar” specimens. This points out that a damage-tolerant design of a 3x3 specimen (or a component with a larger number of cells) starting from the defect volume distribution assessed by considering “1 cell”, “2 cells” or a generic volume extracted from a bar, is expected to be equally effective. However, due to the large scatter of the ECDFs for small volumes, visible in Fig. 8a, a conservative or an unsafe (with respect to the validation specimen) distribution of the defect volume can be randomly obtained, thus affecting the following design stage with numerical models. This result is also confirmed by Fig. 8b, with the estimated histograms characterized by similar trends. The magnified view, on the other hand, shows that the defects with the largest volumes are found in 3x3 specimens. The Gumbel plot in Fig. 8c focuses on the largest defects, which mostly affect the mechanical response [45]. The experimental data on the Gumbel plot for the “1 cell”, “2 cells” and “3x3” specimens show an asymptotic trend and, for this reason, a Type 3 GEV has been considered for the fitting process. In particular, the “3x3” specimen shows an asymptote close to $5 \cdot 10^6$ μm^3, pointing out that defects larger than this upper threshold are not expected to occur. For the “1 cell” and the “2 cells” defects, an asymptotic trend is suggested by the experimental data, but is less evident, since more data are required to confirm the correct value above $4 \cdot 10^6$ μm^3. In particular, the upper threshold obtained by fitting the “2 cells” defect volumes is more accentuated and closer to the one observed for the 3x3 specimens. Accordingly, for the volume feature, it can be concluded that defect inspections in a unit cell are representative of the defect volume population and can be considered for the design, but they do not allow to reliably assess the asymptotic trend for the largest defects. By increasing the number of cells, the upper tail of the largest defect volumes is expected, on the other hand, to be found more reliably. For the bar, the largest defect volume data have been interpolated with a LEVD, since it provides the best fitting with respect to that obtained with the Type 3 GEV. Accordingly, even if the trend is the same for defect volume data below $3 \cdot 10^6$ μm^3, micro-CT inspections on volumes extracted from a bar do not provide indications on a possible asymptotic trend. One solution to overcome this issue may be considering the beam volume as the upper threshold, but this solution can be conservative.

Fig. 9 shows the same plots reported in Fig. 8, but by considering the defect surface. Fig. 9a shows the ECDF functions of the defect surfaces. Fig. 9b compares the histogram of the defect surfaces, whereas Fig. 9c plots the largest defect surfaces on the Gumbel plot, together with the estimated statistical distribution functions.

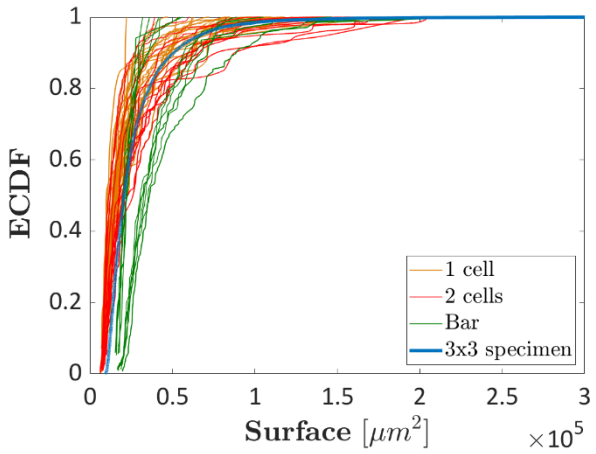

(a)

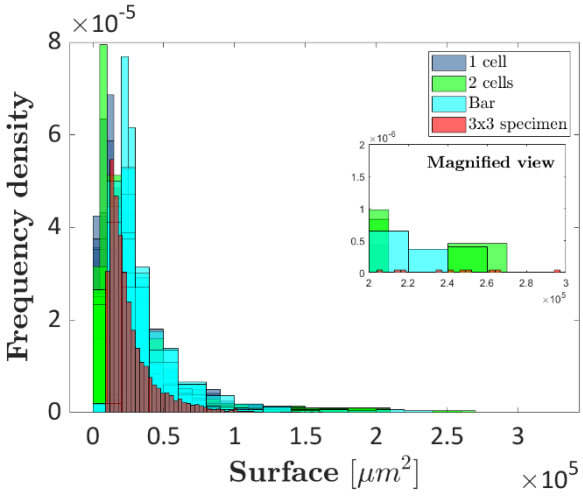

(b)

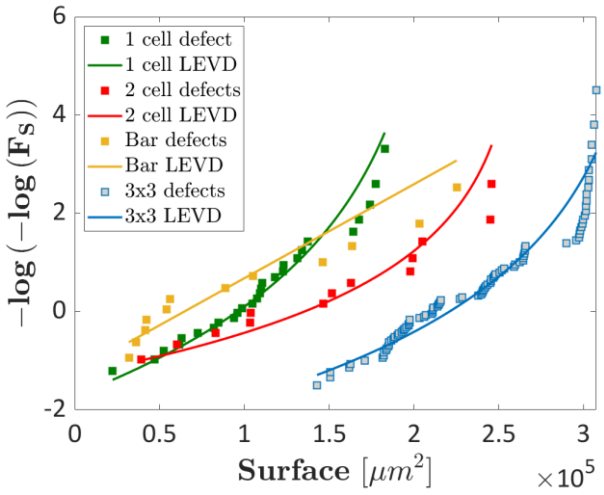

(c)

Figure 9: Analysis of the defect surfaces: a) ECDFs of the defect surfaces; b) histogram plot of the defect surfaces; c) experimental data and estimated functions on the Gumbel plot.

According to Fig. 9a, the trends of the ECDFs obtained by considering the defect surfaces are similar to those obtained by considering the defect volumes, with the "3x3" validation specimen ECDF within the ECDFs for the "1 cell", "2 cells" and "bar" specimens. Analyzing the histogram plot in Fig. 9b and, in particular, the magnified view, it can be noticed that the "2 cells" largest surfaces are close to the "3x3" largest surfaces. On the other hand, by considering the volume (Fig. 8b), the difference between the largest volume in the "3x3" specimen and the other investigated specimens is larger. The analysis of the Gumbel plot provides also interesting results. Indeed, even in this case, the "1 cell" and the "2 cells" data show an asymptotic trend, but this trend is more evident even for the "1 cell" specimens. The slope far from the asymptote is similar, but the curve moves rightward as the investigated number of cells increases. For the surface feature, it is as if an asymptote is found regardless of the investigated number of cells, but this asymptote is smaller in small volumes, suggesting a size effect associated with the number of cells. The difference found by considering the defect volume and the defect surface as the characteristic sizes can be attributed to the morphology of defects, with the ratio surface to volume varying randomly and affecting the resulting distribution.

Fig. 10 shows the same plots reported in Figs. 8 and 9, but by considering the equivalent defect diameter. In particular, in Fig. 10a the ECDFs of the equivalent defect diameters are shown. Fig. 10b compares the histogram of the equivalent defect diameters, whereas Fig. 10c plots the equivalent defect diameters on the Gumbel plot, together with the estimated cumulative distribution functions.

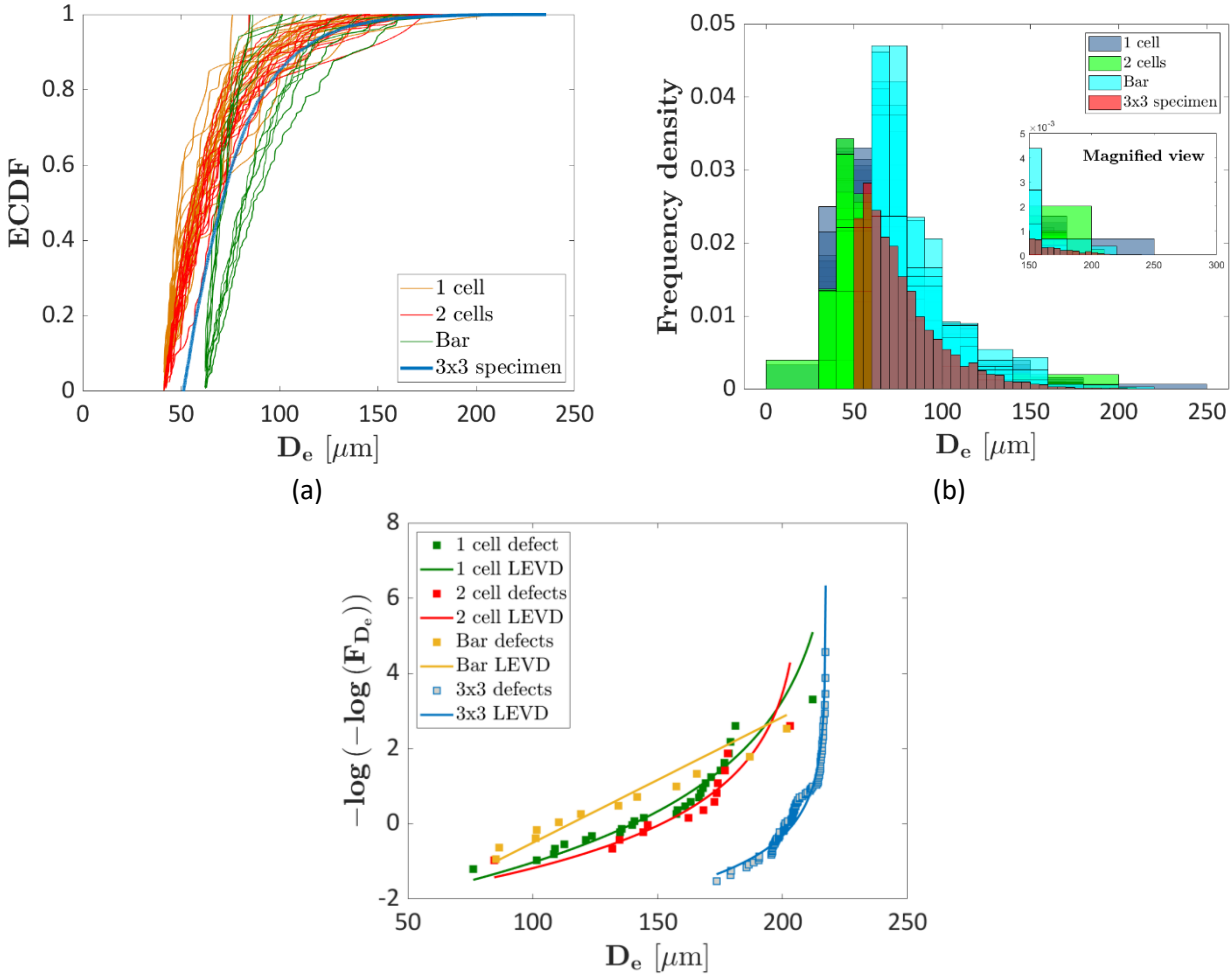

Figure 10: Distribution of defect equivalent diameters: a) ECDFs of the defect equivalent diameters; b) histogram plot of the defect equivalent diameters; c) experimental data and estimated functions on the Gumbel plot.

According to Fig. 10a, the trends of the equivalent diameter ECDFs are similar to the defect volumes and surface ECDF trends, with the "3x3" ECDF within the "1 cell" and the "2 cells" ECDFs. The same considerations hold for the histogram plot in Fig. 10b. However, differently from the histogram plot of the defect volumes, there is not a large difference between the largest equivalent diameter within the "3x3" specimen and the largest equivalent diameters within the "1 cell" and the "2 cells" specimens. According to Fig. 10c, the "1 cell", "2 cells" and "3x3" specimens show an asymptotic trend. The difference between the upper limit threshold found in the "3x3" specimen and the "1 cell" and "2 cells" specimens is limited, differently from Figs. 8c and 9c where the defect volumes and surfaces are considered. For the defects assessed in the bar sub-volumes, even for the equivalent diameter parameter, an asymptotic trend has not been found.

According to these analyses, the equivalent diameter is the characteristic defect size which more reliably models the asymptotic trend even by considering the defect population assessed in a unit cell, i.e., with the smallest difference with respect to the validation specimen. Indeed, this average parameter can be considered less affected by the defect morphology and, accordingly, by the defect surface-to-volume ratios. This analysis has moreover proven that the distribution of defects estimated in a unit cell can be representative of the defect population in specimens with a larger number of cells and can be reliably used for design methodologies based on the entire defect population, as the one developed in [43]. However, it must be considered that conservative or unsafe estimation of the defect population can be assessed by considering

a unit cell, according to the ECDFs reported in Figs. 8a, 9a, 10a, since the assessed population is characterized by large variability. On the other hand, design methodologies based on the largest and most critical defects may be too conservative if the Type 3 GEVD parameters are estimated by considering unit cells, since not capable of properly estimating the asymptote that is clearly visible in the validation specimen.

4. FINITE ELEMENT ANALYSES

In this Section, the numerical activity involving Finite Element Analyses (FEAs) is described. In Section 4.1, the Finite Element model of the lattice structure specimen is described. In Section 4.2, the influence of the characteristic defect parameter is investigated, whereas Section 4.3 focuses on the influence of the defect distribution on the compressive response.

4. 1 Finite Element analyses: model description

Following the approach proposed by the authors in [43], FEAs are carried out to replicate the quasi-static compression tests described in Section 2. The FEA proposed in [43] allows to account for the degrading effect of the defects population in the lattice specimens. Although using 1D beam elements, whose computational effort is significantly smaller than that required by 3D tetra/hexa elements, the model allows to account for the material defectiveness by reducing the nominal diameter of the beam elements according to the characteristic defect size and its distribution within the specimen. Although not determining the actual stress and strain fields in correspondence of the defects, as the defects morphology is not accounted for, the methodology has been shown able to model the degradation of the mechanical response due to internal defects[43] As such, the numerical modelling strategy is particularly appropriate to determine the equivalent defect size which can be more reliably employed for the assessment of the structural integrity of lattice structure specimens under compression loads. In the following, the comparison of three investigated characteristic defect sizes is addressed to identify the most appropriate characteristic defect size in a structural integrity framework. In particular, for the defect surface and volume, the square root and the cubic root are retained as characteristic defect size. Furthermore, FE results obtained with the defect populations estimated from the bar volumes, from the single cell and from each 3x3 lattice specimens are compared to investigate the influence of the retained defect distribution and size effect.

For what concerns the FE model, each beam element has a length of 1 mm, according to a mesh sensitivity analysis conducted in Ref.[43] and the nominal diameter of each node of the beam element, here equal to 1.325 mm according to micro-CT and SEM investigations, is reduced by the defect characteristic size. In a dedicated MATLAB code, nodes are randomly listed, defects are assigned to each node according to their occurrence experimentally assessed through the micro-CT scans, and the diameters of the defective nodes are determined as the difference between the nominal beam diameter and the defect size. According to [43], the influence on the mechanical response of the defect location in the specimen is accounted for by randomly varying the location of the flaws and iteratively repeating the numerical simulations, which also allows to identify a lower-bound design curve through statistical considerations for damage-tolerant designs.

Fig. 11 shows the FE model simulated in the LS-Dyna environment, where the different beam colours highlight that each beam belongs to a dedicated part, whose nodal diameters are different from each other and are defined in accordance with the assigned defects.

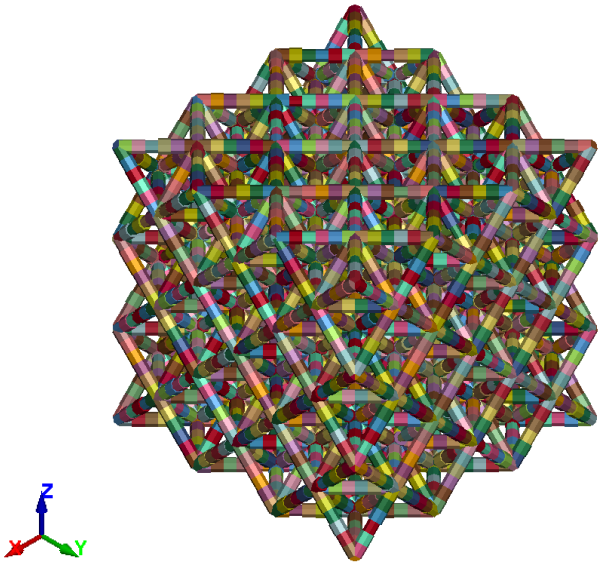

Figure 11: Finite Element model of the lattice specimens with variable diameters in accordance with the defect size distribution assessed with micro-CT inspections.

The material behaviour is modelled through an elasto-plastic material law, whose characteristics have been determined by performing tensile tests on AlSi10Mg bar specimens manufactured with the same parameters of the lattice specimens. The resulting stress-strain curve is reported in Figure 12, while the main parameters are listed in Table 3.

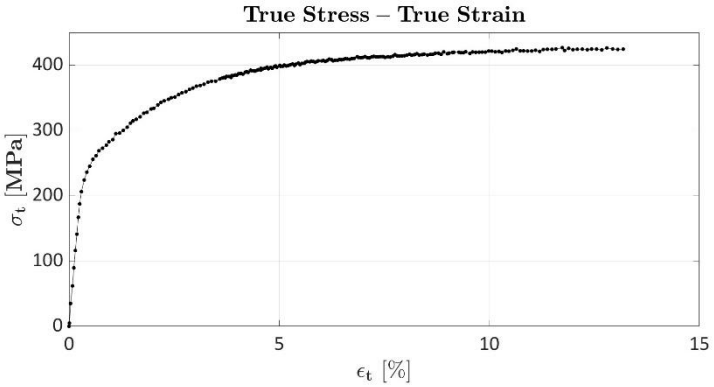

Figure 12: True stress-true strain curve of the tested AlSi10Mg alloy.

Property	Value	Unit
Young's modulus	72	GPa
Yield strength	220	MPa
Ultimate strength	425	MPa
Ultimate strain	0.132	[-]

Table 3: Material properties of the tested AlSi10Mg alloy.

According to Table 3, the Young's modulus of the material is equal to 72 GPa. However, the Young's modulus has been here reduced to account for the influence of strut roughness and manufacturing imperfections which affect the material involved in the mechanical deformation and, accordingly, the elastic response [49]. In LS-Dyna, the *MAT_PIECEWISE_LINEAR_PLASTICITY [50] which also allows to specify a *fail* parameter for element failure and deletion, here assumed equal to the ultimate strain, has been retained. The compressive tests are replicated by considering two rigid walls, one fixed and one moving with a linear displacement law. Contact between beams and rigid walls has been defined with *CONTACT_AUTOMATIC_GENERAL [51].

4.2 Influence of the characteristic defect size

In this section, the three investigated characteristic defect sizes, namely the equivalent diameter, the square root of the defect surface and the cubic root of the defect volume, are compared. All defects detected in the three specimens are accounted for. In order to assess the influence of the defect location on the mechanical response, five numerical simulations are performed by randomly varying the location of the defects in the specimen. The 95% confidence interval is determined by assuming a Normal distribution of the obtained

responses. Figure 13 shows the comparison of the experimental and numerical results with the three characteristic defect sizes.

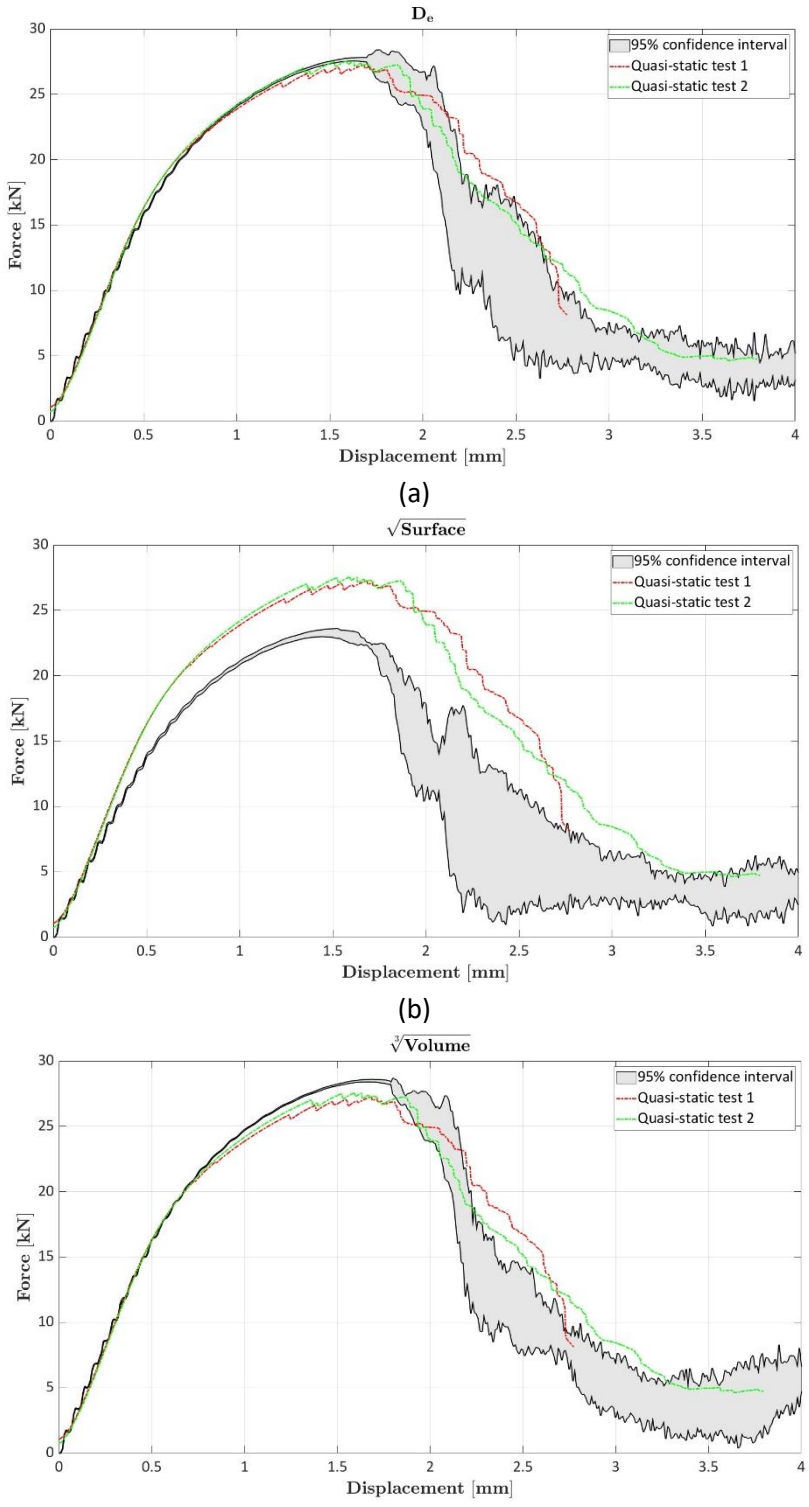

Figure 13. Comparison of experimental data of the compressive tests on the lattice structure specimens and numerical results for different characteristic defect sizes: a) equivalent diameter; b) square root of defect surface; c) cubic root of defect volume.

The equivalent diameter and the cubic root of the defect volume provide similar results both in terms of mean values and in terms of data scatter, while the square root of the defect surface strongly overestimates the degrading effect of the defect. Indeed, the equivalent diameter and the cubic root of the defect volume

represent similar defect characteristics, being the first the diameter of the equivalent sphere and the second the side of the equivalent cube. On the contrary, the square root of the defect surface instead overestimates the defect size being the side of the equivalent square.
As for the data scatter, the equivalent diameter and the cubic root of the defect volume provide similar confidence intervals beyond the peak force, which are also smaller than those obtained by considering the square root of the defect surface. For all three characteristic defect sizes, the data scatter is null in the elastic field and very limited if not null in correspondence of the peak force. Although in accordance with the experimental results, this aspect will be further investigated in the next section.
The equivalent diameter or the cubic root of the defect volume can be considered appropriate parameters to characterize the defect size and its influence on the mechanical response of lattice structures. It must be noted that these results are general, but can be considered mainly valid for the developed approach involving the reduction of the truss section in beam-based lattice structures modeled with 1D elements. With other approaches, the characteristic defect size to be considered should be verified and validated.

The role of small interacting defects must be also discussed. Clusters of small defects may be detrimental to the mechanical response, as well as large defects. The developed procedure is based on the defect analysis carried out in the VG Studio software, which provides the defect distribution, by selecting a threshold which automatically discriminates if a feature is a defect or an artefact. This threshold lets the software search for defects in a defined range of grey-value colors, as detailed in Sections 2 and 3. If the minimum distance between two small defects is smaller than the tomography resolution (25 microns in the present activity), these defects are grouped and considered a unique defect. Otherwise, they are considered as two single defects.

Accordingly, close defects are considered a single defect or separate defects not interacting with each other. It is worth noting that this simplification can affect the analysis of defects in terms of quantity, but it has a negligible effect on the compressive response and, in general, on the structural integrity. Indeed, according to the FE analyses, very large defects affect the compressive response. If a cluster of small defects is present in a critical region, the resulting force-displacement curve may shift downwards, but this shift is limited. Moreover, with the iterative approach followed in the present paper, a range for the experimental curves is obtained. Accordingly, the variability induced by clusters of defects or close interacting defects is expected to be included within this estimated range. This is a strength of the proposed methodology since, even if based on a simplified FE model and the defect characteristic size is modeled by considering one specific feature, it can model the variability of the experimental response, with high-reliability quantile curves which can be considered for the design of components.

According to the analyses carried out in this Section, it has been shown that the investigated defect features are not independent, providing different FE results. It is worth noting that coupling the information on the defect features is expected to provide results that are closer to the experimental results. However, an approach based on coupling the defect features would require more complex simulations with FE models with 3D elements and consequent significantly higher computational efforts. The analyses with 3D models can be employed for specimens but are not feasible for components which are composed of several unit cells. On the other hand, with the approach developed in the present paper, the approximation of considering only one defect feature and 1D elements is counterbalanced by acceptable computational efforts and, for this reason, can be reliably employed even for the design of parts with several repeated unit cells. The information obtained with the analysis of the defect population and in this Section can be exploited to select the most appropriate defect feature for FE models.

4.3 Influence of defect distributions: bar, single cell and full specimen

In this section, the effect of the retained defect distribution is addressed by comparing the results obtained with the defect distributions assessed in the bar specimen, in the single unit cell and in each lattice specimen.

For all distributions, the equivalent diameter is retained as the characteristic defect size. The bar specimen were divided into 12 sub-volumes and 12 different defect distributions were obtained. 12 numerical simulations, one for each defect distribution, were accordingly performed. The lattice specimen consists of 27 unit-cells. For each one, the defect population has been considered in the FE model. Accordingly, 27 numerical simulations were performed. Finally, the defect distributions of each scanned lattice specimen were considered and 3 numerical simulations have been performed.

Fig. 14 shows the obtained results with the different defect distributions in comparison with the experimental data.

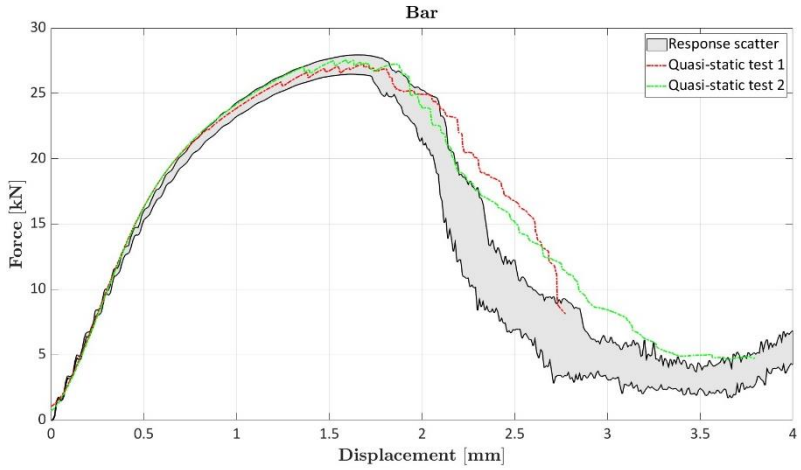

(a)

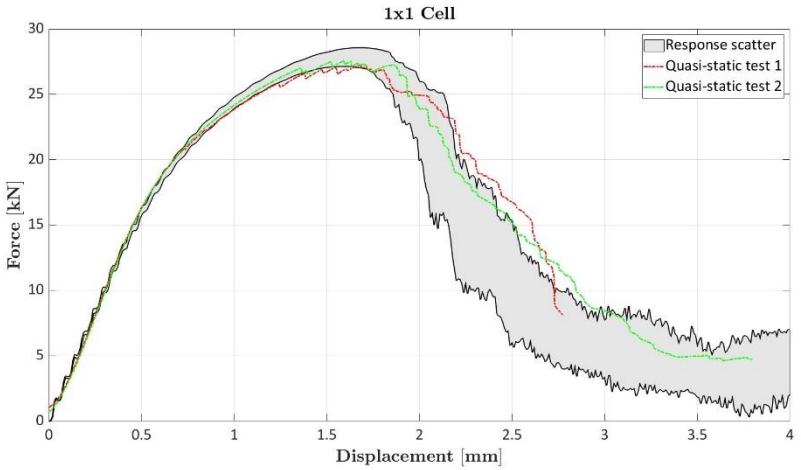

(b)

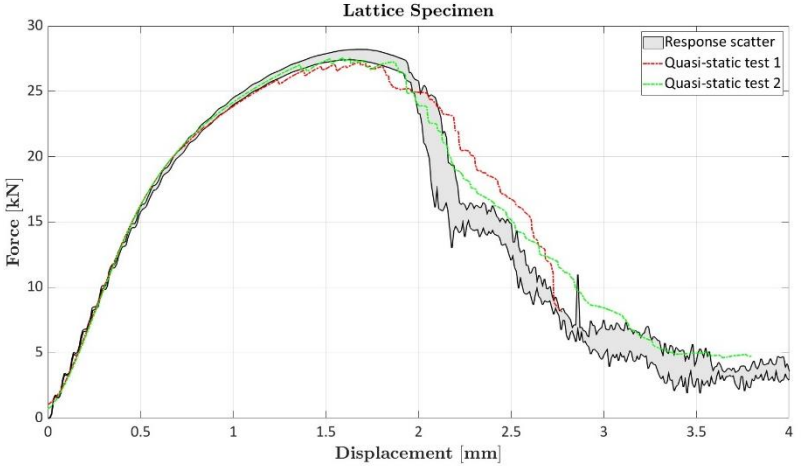

(c)

Figure 14. Comparison of experimental data of the compressive tests on the lattice specimens and numerical results for different defects distributions: a) bar distributions; b) unit-cells distributions; c) 3x3 lattice structure specimen distributions.

In Fig. 14, the grey band corresponds to the scatter of the data and has been obtained from the highest and the lowest responses. All distributions provide results that are in good agreement with the experimental data. However, the data scatter strongly depends on the retained distribution, being consistently higher in the case of the bar and unit-cells distributions with respect to that obtained with the lattice specimen distributions. This can be explained by considering that the distributions obtained in the bar and in the single unit cells are strongly different from each other, while those of the specimens were comparable. As observed in the previous section, the data scatter increases beyond the peak force. However, differently from the results obtained in the previous section, a scatter in the elastic field and in the peak force can be observed, being more pronounced in the case of the defects distributions obtained in the bar and in the unit cells, while limited but evident in the case of the defects populations determined from each lattice specimen. In combination with the results of the previous section, it can be argued that: i) the elastic field and the peak force depend on the maximum defect size, which varies within the retained distributions, but not on its position within the specimen, as observed in the previous section; ii) the scatter of the response beyond the peak force is influenced both by the location of defects within the specimen and by the retained defect distribution, as evidenced in Fig. 14.
Finally, the results of this analysis show that the defect populations obtained on the bar specimens can be retained in the proposed FEA to evaluate the influence of the material defectiveness on the compressive response of lattice structures. However, by considering also the statistical analyses in Section 3, assessing the defect population in lattice structure specimens, even if with a number of cells smaller than that of the component to be designed, is suggested.

These analyses have further proven the effectiveness of micro-CT analyses, combined with finite element simulations, as a non-destructive technique for assessing the structural integrity of AM parts with complex geometries, like lattice structures. Further useful information on the damage evolution and the origin of failure can be obtained with in-situ tests[52] or time lapse in situ X-ray imaging of failure[53] and can be considered a further development of this research activity.

It must be noted that the results obtained in the present paper are general and provide useful indications on the influence of defects on the compressive response and, in general, on the structural integrity of lattice structures. However, defects are strongly dependent on the AM material and initial powder quality, process parameters, the lattice geometry and the interactions between the last two factors. Accordingly, the defect feature to be considered as the characteristic defect size is suggested to be verified if the material or the process parameters are changed. Indeed, even if three specimens have been inspected and a large amount of defects have been investigated, the variation of the mechanical response of AM parts can be large and an experimental validation is suggested when a new set of material – process parameters – lattice geometry is considered. Moreover, the simplified FE model can be employed only for beam lattice structures, and not for other types of lattice structures, like gyroid lattice structures. However, the proposed approach and methodology for the assessment of the influence of internal defects is general and can be replicated regardless of the cell type and process parameters, provided that an appropriate simplified model is developed. Moreover, it has been proven that the defect population can be assessed in a rectangular bar or, in general, in specimens with standard geometry. According to Section 3, conservative results are obtained, since the investigated largest defect features obtained from a bar do not follow an asymptotic trend.

The results obtained in the present research activity provide useful indications for the design of lattice structures and for modelling the experimental scatter induced by manufacturing defects. The experimental-

numerical procedure developed has been applied by considering an octet-truss lattice structure, but it can be reliably exploited also for other types of cells.

5. SUMMARY

In the present work, the influence of defects on the compressive response of lattice structure specimens is investigated. The defect population was assessed with micro-CT analyses carried out on AlSi10Mg cubic lattice structure specimens composed of 27 octet unit cells, three on each side, produced with a Selective Laser Melting (SLM) process. The defect population in the whole specimens and in 27 unit cells, in 13 volumes corresponding to the volume of two unit cells and in volumes extracted from a rectangular bar was considered in the analysis. Numerical simulations were thereafter carried out to simulate the experimental compressive tests..

The following conclusions can be drawn:

a) The defect distribution assessed on unit cells can be representative of the defect population of the whole specimen. However, relying on single cells or a limited number of cells for the assessment of the defect population may also provide non-conservative defect populations, thus affecting the structural integrity of the part to be designed. .
b) The largest and most critical defects have been analyzed by considering the Statistics of Extreme Values (SEV). The statistical distributions estimated by considering the lattice structure specimens or one or two cells show a linear increasing trend ending with an asymptote. On the other hand, the distribution estimated starting from the volume extracted from the bar shows a continuously increasing trend and therefore it is not suggested in design procedures based on the largest extreme defects.
c) The defect characteristic size should be carefully selected when modelling lattice structure specimens. The equivalent diameter has proven to be the most effective parameter for the investigated specimens, allowing for a simulation of the compressive response closest to the experimental results.
d) The defect populations obtained by considering the bar volumes are comparable to those extracted by considering a unit cell and the specimen with 27 cells and, accordingly, can be retained in the developed Finite Element (FE) modelling methodology assessing the influence of the material defectiveness on the compressive response. However, according also to the results of the statistical analyses, the assessment of the defect population is suggested in specimens made of lattice structure, even in a unit cell.

To conclude, the analyses carried out in the paper provide important general indications for the design of lattice structures with numerical models accounting also for the influence of defects. These results, however, should be verified case by case, since the defect population strongly varies with the AM process parameters and the cell geometry. However, the design-oriented strategy employed in the paper, based on micro-CT inspections and following simulations accounting for the influence of defect size by considering the defect equivalent diameter, independent from the beam and the stress orientations, can be generalized and employed even for cells with different geometries, providing reliable results with limited computational efforts.

REFERENCES

1 Gunasegaram DR, Steinbach I. Modelling of microstructure formation in metal additive manufacturing: Recent progress, research gaps and perspectives. *Metals (Basel)*. 2021;11: 1–19.

2 Bajaj P, Hariharan A, Kini A, Kürnsteiner P, Raabe D, Jägle EA. Steels in additive manufacturing: A review of their microstructure and properties. *Mater Sci Eng A*. 2020;772.

3 Li N, Huang S, Zhang G, Qin R, Liu W, Xiong H. Journal of Materials Science & Technology Progress in additive manufacturing on new materials : A review. *J Mater Sci Technol*. 2019;35: 242–269.

4 Sanaei N, Fatemi A. Defects in additive manufactured metals and their effect on fatigue performance: A state-of-the-art review. *Prog Mater Sci*. 2021;117: 100724.

5 Brennan MC, Keist JS, Palmer TA. Defects in Metal Additive Manufacturing Processes. *J Mater Eng Perform*. 2021;30: 4808–4818.

6 du Plessis A, Yadroitsava I, Yadroitsev I. Effects of defects on mechanical properties in metal additive manufacturing: A review focusing on X-ray tomography insights. *Mater Des*. 2020;187: 108385.

7 Kempen K, Thijs L, Humbeeck J Van, et al. Processing AlSi10Mg by selective laser melting : parameter optimisation and material characterisation Processing AlSi10Mg by selective laser melting : parameter optimisation and material characterisation. 2015;0836.

8 Seifi M, Dahar M, Aman RON, Harrysson OLA, Beuth J, Lewandowski JJ. Evaluation of Orientation Dependence of Fracture Toughness and Fatigue Crack Propagation Behavior of As-Deposited ARCAM EBM Ti-6Al-4V. 2015;67: 597–607.

9 Baig S. Tensile and fatigue behaviors of additively manufactured AlSi10Mg : Effect of solutionizing and aging heat treatments. 2023: 2662–2680.

10 Aboulkhair NT, Maskery I, Tuck C, Ashcroft I, Everitt NM. Materials Science & Engineering A The microstructure and mechanical properties of selectively laser melted AlSi10Mg : The effect of a conventional T6-like heat treatment. *Mater Sci Eng A*. 2016;667: 139–146.

11 Li W, Li S, Liu J, et al. Materials Science & Engineering A Effect of heat treatment on AlSi10Mg alloy fabricated by selective laser melting : Microstructure evolution , mechanical properties and fracture mechanism. *Mater Sci Eng A*. 2016;663: 116–125.

12 Ghio E. Additive Manufacturing of AlSi10Mg and Ti6Al4V Lightweight Alloys via Laser Powder Bed Fusion : A Review of Heat Treatments Effects. 2022.

13 Gockel J, Sheridan L, Koerper B, Whip B. The in fl uence of additive manufacturing processing parameters on surface roughness and fatigue life. *Int J Fatigue*. 2019;124: 380–388.

14 Masuo H, Tanaka Y, Morokoshi S, et al. Influence of defects, surface roughness and HIP on the fatigue strength of Ti-6Al-4V manufactured by additive manufacturing. *Int J Fatigue*. 2018;117: 163–179.

15 Yánez A, Paula M, Cuadrado A, Martel O, Monopoli D. Surface roughness e ff ects on the fatigue behaviour of gyroid cellular structures obtained by additive manufacturing. *Int J Fatigue*. 2020;138: 105702.

16 Tridello A, Fiocchi J, Biffi CA, et al. Effect of microstructure, residual stresses and building orientation on the fatigue response up to 109 cycles of an SLM AlSi10Mg alloy. *Int J Fatigue*. 2020;137.

17 Jiang Z, Sun J, Berto F, Wang X, Qian G. Fatigue and Fracture Behavior of AlSi10Mg Manufactured by Selective Laser Melting : A Review. 2023;26: 367–390.

18 Beretta S, Romano S. A comparison of fatigue strength sensitivity to defects for materials manufactured by AM or traditional processes. *Int J Fatigue*. 2017;94: 178–191.

19 Sanaei N, Fatemi A. Defects in additive manufactured metals and their effect on fatigue performance: A state-of-the-art review. *Prog Mater Sci*. 2021;117: 100724.

20 Ferro P, Fabrizi A, Berto F, Savio G, Meneghello R, Rosso S. Defects as a root cause of fatigue weakening of additively manufactured AlSi10Mg components. *Theor Appl Fract Mech*. 2020;108: 102611.

21 Zhu J, Zhou H, Wang C, Zhou L, Yuan S. A review of topology optimization for additive manufacturing : Status and challenges. *Chinese J Aeronaut*. 2021;34: 91–110.

22 Boursier Niutta C, Tridello A, Barletta G, et al. Defect-Driven topology optimization for fatigue design of additive manufacturing structures: Application on a real industrial aerospace component. *Eng Fail Anal*. 2022;142: 106737.

23 Liu J, Gaynor AT, Chen S, et al. Current and future trends in topology optimization for additive manufacturing. *Struct Multidiscip Optim*. 2018;57: 2457–2483.

24 Pan C, Han Y, Lu J. Design and optimization of lattice structures: A review. *Appl Sci*. 2020;10: 1–36.

25 Maconachie T, Leary M, Lozanovski B, et al. SLM lattice structures : Properties , performance , applications and challenges. *Mater Des*. 2019;183: 108137.

26 Obadimu SO, Kourousis KI. Compressive Behaviour of Additively Manufactured Lattice Structures : A Review. 2021.

27 Alkentar R, Máté F, Mankovits T. Investigation of the Performance of Ti6Al4V Lattice Structures Designed for Biomedical Implants Using the Finite Element Method. *Materials (Basel)*. 2022;15.

28 Sajjad U, Rehman T ur, Ali M, Park CW, Yan WM. Manufacturing and potential applications of lattice structures in thermal systems: A comprehensive review of recent advances. *Int J Heat Mass Transf*. 2022;198: 123352.

29 Camilo D, Sierra M, Astaraee AH, Guagliano M, Bagherifard S. Numerical Investigation of Ti6Al4V Gradient Lattice Structures with Tailored Mechanical Response. 2022;2101760.

30 Uddin MA, Barsoum I, Kumar S, Schiffer A. Enhancing compressive performance in 3D printed pyramidal lattice structures with geometrically tailored I-shaped struts. *Mater Des*. 2024;237: 112524.

31 Nugroho WT, Dong Y, Pramanik A, Chithirai Pon Selvan M, Zhang Z, Ramakrishna S. Additive manufacturing of re-entrant structures: Well-tailored structures, unique properties, modelling approaches and real applications. *Addit Manuf*. 2023;78: 103829.

32 Niutta CB, Ciardiello R, Tridello A. Experimental and Numerical Investigation of a Lattice Structure for Energy Absorption: Application to the Design of an Automotive Crash Absorber. *Polymers (Basel)*. 2022;14.

33 Iqbal A, Nasrullah H, Puji S, Dirgantara T. Design and optimization of crashworthy components based on lattice structure configuration. *Structures*. 2020;26: 969–981.

34 Hou W, He P, Yang Y, Sang L. International Journal of Mechanical Sciences Crashworthiness optimization of crash box with 3D-printed lattice structures. *Int J Mech Sci*. 2023;247: 108198.

35 Wang X, Qin R, Chen B. Materials & Design Laser-based additively manufactured bio-inspired crashworthy structure : Energy absorption and collapse behaviour under static and dynamic loadings. *Mater Des*. 2021;211: 110128.

36 Wang Y, Chang C, Liu P, Lin C. Feasibility evaluation of a new lattice for porous surface design in additive manufacturing medical implants under interfacial tensile bonded testing. *Addit Manuf*. 2023;66: 103455.

37 Alomar Z, Concli F. A Review of the Selective Laser Melting Lattice Structures and Their Numerical Models. 2020;2000611: 1–17.

38 Cao X, Jiang Y, Zhao T, et al. Compression experiment and numerical evaluation on mechanical responses of the lattice structures with stochastic geometric defects originated from additive-manufacturing. *Compos Part B*. 2020;194: 108030.

39 Benedetti M, Plessis A, Ritchie RO, Dallago M, Razavi N, Berto F. Materials Science & Engineering R Architected cellular materials : A review on their mechanical properties towards fatigue-tolerant design and fabrication. *Mater Sci Eng R*. 2021;144: 100606.

40 Jiang P, Meter EC De, Basu S. The influence of defects on the elastic response of lattice structures resulting from additive manufacturing. *Comput Mater Sci*. 2021;199: 110716.

41 Rodríguez-Aparicio R, Alegre JM, Verbeeten WMH, Lorenzo-Bañuelos M, Cuesta II. Methodology to predict mechanical properties of PA-12 lattice structures manufactured by powder bed fusion. *Addit Manuf*. 2023;78.

42 Carlton HD, Volkoff-shoemaker NA, Messner MC, Barton NR. Materials Science & Engineering A Incorporating defects into model predictions of metal lattice-structured materials. *Mater Sci Eng A*. 2022;832: 142427.

43 Boursier Niutta C, Paolino DS, Tridello A. Additively manufactured lattice structures: An innovative defect-based design methodology against crash impact. *Eng Fail Anal*. 2023;152: 107436.

44 della Ripa M, Paolino DS, Amorese A, Tridello A. Numerical modelling of the mechanical response of lattice structures produced through AM. *Procedia Struct Integr*. 2021;33: 714–723.

45 Murchio S, Dallago M, Zanini F, et al. Additively manufactured Ti–6Al–4V thin struts via laser powder bed fusion: Effect of building orientation on geometrical accuracy and mechanical properties. *J Mech Behav Biomed Mater*. 2021;119: 104495.

46 Murakami Y. *Metal Fatigue: Effects of Small Defects and Nonmetallic Inclusions*. Elsevier; 2002.

47 Colombo C, Tridello A, Pagnoncelli AP, et al. Efficient experimental methods for rapid fatigue life estimation of additive manufactured elements. *Int J Fatigue*. 2023;167: 107345.

48 Beretta S. More than 25 years of extreme value statistics for defects: Fundamentals, historical developments, recent applications. *Int J Fatigue*. 2021;151: 106407.

49 Suard M, Martin G, Lhuissier P, et al. Mechanical equivalent diameter of single struts for the stiffness prediction of lattice structures produced by Electron Beam Melting. *Addit Manuf*. 2015;8: 124–131.

50 LSTC. (2017b). LS-DYNA Keyword User's Manual Volume II.

51 LSTC. (2017a). LS-DYNA Keyword User's Manual Volume I.

52 Wu W, Qi D, Hu W, et al. Synchrotron X-ray micro-computed tomography imaging of 3D re-entrant micro lattice during in situ micro compression experimental process. *Mater Des*. 2020;192.

53 Qian W, Wu S, Lei L, Hu Q, Liu C. Time lapse in situ X-ray imaging of failure in structural materials under cyclic loads and extreme environments. *J Mater Sci Technol*. 2024;175: 80–103.